Crystal field and Kondo effects in $CeCu_6$ and $CeAl_3$

S. P. Strong*
Theoretical Physics-Oxford University, 1 Keble Road, Oxford, OX3 7RJ United Kingdom

A. J. Millis
AT&T Bell Laboratories, Murray Hill, New Jersey 07974

(Received 12 January 1994; revised manuscript received 21 July 1994)

We calculate the temperature dependence of the specific heat, susceptibility, and resistivity for an isolated cerium ion in crystal-field environments appropriate for the cerium sites in $CeCu_6$ and $CeAl_3$. We use the self-consistent ladder approximation for intermediate and high temperatures and match to exact results to obtain low-temperature behavior. We find unusual temperature dependence for all the calculated quantities as a result of the competition between crystal-field effects and the Kondo effect. Our results for specific heat and susceptibility agree well with the data, except that the independent ion approximation predicts somewhat smaller Wilson ratios than observed, perhaps implying weak ferromagnetic correlations. The resistivity is not well reproduced.

I. INTRODUCTION

The goal of this paper is to determine exactly how much of the temperature dependence and magnitude of various experimentally measurable properties of $CeAl_3$ and $CeCu_6$ can be understood within a model of independent cerium ions treated as local moments Coqblin-Schrieffer[1] coupled to a bath of itinerant electrons. The literature is unclear on this point because the interplay between crystal fields and the Kondo effect in these materials has not been quantitatively addressed over a range of temperatures. The physical quantities that we calculate are the specific heat, the static magnetic susceptibility, the imaginary part of the susceptibility at finite frequency, and the resistivity. In our calculation, unusual temperature dependences, similar to those observed experimentally, arise in all of these quantities as a result of the competition between crystal-field effects and the Kondo effect.

In this paper we assume that the Ce ion has the valence configuration $4f_1$, i.e., that the f shell contains one electron, and that the spin-orbit coupling allows us to restrict our attention to the $J=\frac{5}{2}$ multiplet. The characteristic energy scale for charge fluctuations and for transitions to the $J=\frac{7}{2}$ multiplet are believed to of the order of 3000 K (Ref. 2), too high to be relevant to our calculations. The six states of the $J=\frac{5}{2}$ multiplet, which we consider, are further split into three doublets by crystal-field effects; the crystal-field splittings range from 60 to 160 K and are discussed further in Sec. II B. Two other important energy scales are the sixfold Kondo temperature $T_0^{(6)}$, which is the Kondo temperature the $J=\frac{5}{2}$ multiplet would have if the crystal fields vanished, and $T_0^{(2)}$, the effective Kondo temperature for the lowest-lying doublet. In the cases we consider $T_0^{(6)} \approx 43$ K, implying strong competition between Kondo and crystal-field effects, but $T_0^{(2)} \sim 3$ K, implying a reasonable separation of energy scales between the quenching of the lowest-lying doublet and the crystal-field–Kondo elimination of the higher doublets. The various energy scale scales are sketched in Fig. 1.

The calculations are done using the self-consistent ladder approximation (SCLA) introduced by Maekawa *et al.*[2] as an extension of Abrikosov's original pseudofermion treatment of the Kondo problem[3] to more complicated models of magnetic impurities. The formalism leads to a set of coupled integral equations from whose solution various physical quantities may be calculated. The resummation is known to give unreliable results at sufficiently low temperatures but is believed to have a wide range of applicability, extending even below the appropriate Kondo temperature scales for the models to which it has been applied.[4] To extrapolate physical properties down to lower temperatures, we match SCLA results at the higher temperatures to exact results for the

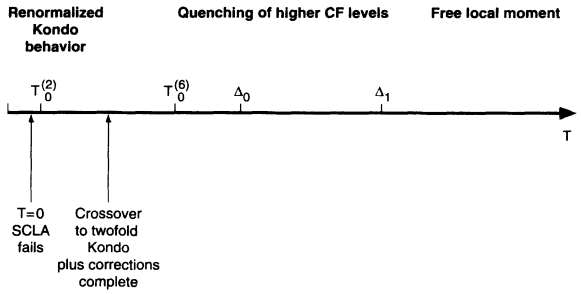

FIG. 1. Sketch of relevant energy scales for our model. For $CeAl_3$ the crystal field levels are at 60 and 90 K, the sixfold Kondo temperature $T_0^{(6)}$ is 43 Kelvin, the effective twofold Kondo temperature $T_0^{(2)}$ is 3.6 K and the twofold Kondo behavior plus corrections is observed below 15 K. For $CeCu_6$ the crystal-field levels are at 80 and 160 K, the sixfold Kondo temperature $T_0^{(6)}$ is 43 K, the effective twofold Kondo temperature $T_0^{(2)}$ is 3.2 K, and the twofold Kondo behavior plus corrections is observed below 15 K.

Kondo model as described in detail in the text.

The outline of the paper is as follows. In Sec. II we introduce the model Hamiltonian we will study and describe the self-consistent ladder approximation and how its results may be extrapolated to low temperatures. The actual calculations of physical quantities are presented as needed in subsequent sections. In Sec. III we calculate the zero-frequency susceptibility for a cerium ion in crystal-field environments appropriate to $CeAl_3$ and $CeCu_6$ and compare our results with experiment. In Sec. IV we calculate the specific-heat contributed by a single cerium ion and compare our results with experimental results for $CeAl_3$ and $CeCu_6$. In Sec. V we calculate the imaginary part of the static susceptibility at finite temperature and compare with neutron-scattering results. In Sec. VI we calculate the temperature dependence of the resistivity for $CeAl_3$ and $CeCu_6$ for free-electron dispersion in the conduction band and compare with experimental results. Finally, in Sec. VII we summarize our results and draw conclusions from the comparisons with experiment.

II. THE MODEL HAMILTONIAN

A. The self-consistent ladder approximation

Our Hamiltonian is

$$H=\sum_m E_m f_m^\dagger f_m+\sum_{k,m}\epsilon_k c_{km}^\dagger c_{km} -J\sum_{k,k'}\sum_{m,m'} f_{m'}^\dagger f_m c_{km}^\dagger c_{k'm'} . \quad (1)$$

The f operators create and annihilate electrons in the $J=\frac{5}{2}f$ subspace, and the m labels designate particular superpositions of the $J=\frac{5}{2}$ states, which are energy eigenstates, with energies E_m, in the presence of crystal-field effects. The c operators represent the conduction-band-electron creation and annihilation operators, and are labeled by a radial wavevector k and by m. We have assumed that the coupling of the $4f$ state to the conduction band is k independent and of the Coqblin-Schrieffer form.

The Hamiltonian must be supplemented by the constraint

$$\sum_m f_m^\dagger f_m=1 \quad (2)$$

to ensure that the local moment is represented correctly, or, equivalently, that we include only the physically relevant $4f_1$ configuration. The f operators create and annihilate f electrons and are closely analogous to the physical f-electron creation and annihilation operators. However, because they obey a single occupancy constraint, which allows only pairs of $f^\dagger$ and f operators to appear (never single creation or annihilation operators), we refer to them as pseudofermion operators.

To enforce the constraint, we follow Abrikosov[3] and Maekawa *et al.*[2] and work in the grand canonical ensemble, with a chemical potential, λ, for the f pseudofermions. The expectation value of an operator O in this ensemble is given by

$$\langle O\rangle_\lambda=\sum_n \mathrm{Tr}[O\exp[-\beta(H+n\lambda)]_n/Z_\lambda .$$

The subscript on the trace denotes that it is taken the subspace with n pseudofermions. Z_λ is given by $\sum_n \mathrm{Tr}\{\exp[-\beta(H+n\lambda)]\}_n$. This division into subspaces labeled by n is allowed because the Hamiltonian conserves the number of pseudofermions. The expectation value within the $n=1$ subspace for an operator O can be computed by taking $\lim_{\lambda\to\infty}\exp(\beta\lambda)\partial/\partial\lambda\langle O\rangle_\lambda Z_\lambda$ and dividing by the partition function in the $n=1$ subspace, which is given by the same expression with the identity operator substituted for O. This method of projecting onto the singly occupied subspace had been used before by several authors.[10–12] The formalism can also be used to calculate dynamical quantities, such as correlation functions because the Hamiltonian conserves n, because the projection onto the $n=1$ subspace is preserved at all stages in a calculation.[2,13]

If one is interested in finite temperature and dynamical properties, the Hamiltonian of Eq. (1) is too complicated to treat exactly. There does exist a selective resummation of perturbation theory, which has been proven to be self-consistent[14] and which is widely used to calculate finite-temperature properties for Hamiltonians of the form of Eq. (1). In the form we will use, the approximation is known as the self-consistent ladder approximation because of the set of diagrams, which it retains for resummation. The approximation is also equivalent to the Coqblin-Schrieffer limit of the noncrossing approximation of Kuramoto.[14]

In this approximation, the f pseudofermion self-energy is calculated by summing the ladder diagrams in which an f pseudofermion interacts repeatedly with a single conduction electron. At all stages the full pseudofermion propagator is used in the ladder, including the self-energy being calculated. The corrections to the conduction-band propagator from a single cerium ion are $O(1/V)$, where V is the volume of the system, and they vanish in the thermodynamic limit. For a finite density of cerium ions, this self-energy does not vanish, and its neglect is an uncontrolled approximation, which implies no correlation between different cerium ions and no average effect on the conduction electrons. For a flat conduction-band density of states $N(0)$ with a hard cutoff D this prescription results in the self-consistent integral equation:[2]

$$\Sigma(i\omega_n)=-JN(0)\int_{-D}^{D}D\epsilon_1 f(-\epsilon_1)\left[1-\left[1+JN(0)\sum_m\int_{-D}^{D}d\epsilon_2 f(\epsilon_2)G_{fm}(i\omega_n+\epsilon_2-\epsilon_1)\right]^{-1}\right], \quad (3)$$

where f is the Fermi distribution function and

$$G_{fm}(i\omega_n)=\frac{1}{i\omega_n-E_m-\Sigma(i\omega_n)} . \tag{4}$$

Note that the self-energy is independent of m. Equation (3) is more conveniently rewritten as two coupled integral equations:

$$\Sigma(i\omega_n)=-JN(0)\int_{-D}^{D}d\epsilon_1\frac{f(-\epsilon_1)\Pi(i\omega_n-\epsilon_1)}{1+\Pi(i\omega_n-\epsilon_1)} , \tag{5}$$

$$\Pi(i\omega_n-\epsilon_1)=JN(0)\sum_m\int_{-D}^{D}d\epsilon_2\frac{f(\epsilon_2)}{i\omega_n-\epsilon_1+\epsilon_2-E_m-\Sigma(i\omega_n-\epsilon_1+\epsilon_2)} . \tag{6}$$

We continue these equations to real ω's and solve them numerically by iteration. An initial guess for $\sum_m G_m$ is made (either corresponding to $\Sigma=0$ or using the result for $\sum_m G_m$ from some previous run to a not too different set of parameters). Π is then calculated by use of Eq. (6) and then G_m is calculated from Π using Eq. (5). This procedure is iterated until the average fractional change in the real and imaginary parts of $\sum_m G_m$ becomes less than a part in 10^8. The integrals are done using the trapezoidal rule. A logarithmic mesh of sampling points is used, with the exception of a small central region of 100 evenly spaced points centered on the sharpest feature in $\mathrm{Im}\{\Pi/[1-JN(0)\Pi]\}$. These points are set $0.4\,JN(0)T$ apart in energy in order to guarantee that the sharpest feature in $\mathrm{Im}\{\Pi/[1-JN(0)\Pi]\}$ is well sampled. The remaining points are distributed, half on each side of the central region extending from the edge of the central region out to twice the bandwidth cutoff D in such a way that the ratio of each step to its predecessor is constant. The same mesh is used for both Π and Σ, since this facilitates the calculation of $\omega=0$ quantities. The program typically converges after two iterations when an initial guess obtained from a similar set of parameters is used and in four or five iterations when the initial guess is taken as $\Sigma\sim 0$. The typical execution time with 500 mesh points was around 30 s per iteration running on a Silicon Graphics Irix computer.

The specific heat, zero-frequency susceptibility, and imaginary part of the finite-frequency susceptibility can all be calculated from the solution. We reserve the discussion of the extraction of particular physical quantities to the sections relating to each quantity. It is, however, convenient at this point to introduce the spectral densities, $\rho_m(x)$ for the pseudofermion Green's function, and $\eta(x)$ for the ladder sum $\Pi(x)/[1+\Pi(x)]$. Since the chemical potential will shift all of the energies by λ, we subtract this energy off in our definition of ρ:

$$\rho_m(x)=-\frac{1}{\pi}\frac{\mathrm{Im}\,\Sigma(i\omega_n\to x+\lambda+i0^+)}{[x-E_m-\mathrm{Re}\,\Sigma(i\omega_n\to x+\lambda+i0^+)]^2+[\mathrm{Im}\,\Sigma(i\omega_n\to x+\lambda+i0^+)]^2} . \tag{7}$$

The subtraction is unnecessary for η:

$$\eta(x)=-\frac{1}{\pi}\frac{\mathrm{Im}\,\Pi(i\omega_n\to x+i0^+)}{[1+\mathrm{Re}\,\Pi(i\omega_n\to x+i0^+)]^2+[\mathrm{Im}\,\Pi(i\omega_n\to x+\lambda+i0^+)]^2} . \tag{8}$$

The quantities $\bar{\rho}_m$,

$$\bar{\rho}_m(h)=\exp(-\beta x)\rho_m(x) , \tag{9}$$

and $\bar{\eta}$,

$$\bar{\eta}(h)=\exp(-\beta x)\eta(x) , \tag{10}$$

are also useful.

Although the approximation we have made by doing a selective resummation of perturbation theory is, in principle, uncontrolled, there are several reasons to believe that it will offer a good quantitative description of the physics of our model. First, the approximation agrees up to order $1/N$ with the $1/N$ expansion for the Coqblin-Schrieffer model. The $1/N$ expansion is believed to be convergent, or at least asymptotic, at zero temperature and over some finite range of nonzero temperatures.[4] Second, the noncrossing approximation, to which the SCLA is equivalent in the Coqblin-Schrieffer limit, has been investigated extensively by a variety of authors.[13,15,4] The approach is known to fail at zero temperature, where it does not correctly reproduce the Fermi-liquid nature of the ground state, but finite-temperature results agree well with exact results down to below the relevant Kondo temperatures.

B. Crystal-field parameters

For $CeAl_3$, the crystal field experienced by the cerium atoms has hexagonal symmetry splitting the $J=5/2$ states into three doublets. We use splittings proposed on the basis of neutron-scattering results:[17] The ground doublet consists of the two $J^z=\pm\frac{3}{2}$ states. The first excited doublet consists of the two $J^z=\pm\frac{5}{2}$ states and lies 60 K above the ground doublet, while the highest doublet, containing the $J^z=\pm\frac{1}{2}$ states, lies at 90 K above the ground doublet. We use a hard cutoff D of 1150 K and set $JN(0)=0.053$. These parameters have been chosen to give a Kondo temperature,[5] $T_0^{(6)}$, of 43 K in the absence of crystal-field splitting,[18] corresponding with the choice of Kawakami, Usuki, and Okiji,[19] who calculate the

zero-temperature magnetization curve and zero-temperature specific-heat coefficient for $CeAl_3$ in a single-site approximation using the Bethe ansatz.[20] This allows us to compare our zero-temperature results with their exact results for $T=0$.

For $CeCu_6$ there are four cerium ions per unit cell. These sit in a complex crystalline environment with no obvious symmetry. Further, although the arrangements of the 19 copper nearest neighbors of each cerium are identical, the orientation of this structure with respect to the crystalline axes is different for the different ceriums. The complexity of this environment leads us to expect no degeneracies for the crystal-field eigenstates other than the twofold degeneracy required by time-reversal invariance. Tentative splittings for the resulting three doublets have been proposed on the basis of neutron-scattering experiments.[21,22] We take the first excited doublet to lie 80-K above the ground state doublet and the highest-lying doublet to lie 160 K higher above the ground state doublet. We choose $JN(0)=0.060$ and $D=1000$ to match the experimental low-temperature specific-heat coefficient for $CeCu_6$. Because of the complexity of the Cerium ion's crystal-field environment, the wave functions for the doublets are not determined by symmetry. We are forced to make an educated guess at suitable wavefunctions and to adopt an approximate procedure for computing the susceptibility. This is described in Sec. III.

For this choice of crystal-field spacings and couplings we expect the higher-lying crystal field states to be strongly hybridized with the low-lying crystal-field states before finally freezing out. The crystal-field splittings are sufficiently large for this freezing out to occur before the Kondo quenching of the lowest-lying doublet, so the low-temperature physics is basically that of the Kondo quenching of the lowest-lying crystal-field doublet but with a renormalized coupling constant and effective moment for the ground-state doublet. On these grounds we expect the following behavior. At high temperatures ($T > 150$ K) one has essentially a free local moment. This is modified at intermediate temperatures ($15\text{ K} < T < 150$ K), where Kondo and crystal-field effects compete, resulting in some complicated crossover behavior. At low temperatures ($T < 15$ K) the behavior crosses over to that of the renormalized Kondo model plus small corrections. The SCLA fails qualitatively at sufficiently low temperatures ($T < 3$ K) but allows us to extract the parameters we need to describe the low energy behavior as previously described. The expected behavior as a function of temperature is shown in Fig. 1. The essential point is that there is a clear separation of scales between the Kondo quenching of the last doublet, which occurs around 3 K and the crystal-field–Kondo elimination of the high-lying crystal field states, which is complete by 20 K. This allows the extrapolation scheme explained in the next section to be applied to the SCLA results to get predictions to low-temperature properties.

C. Extrapolation to low temperatures

At low temperatures the physical properties calculated with the self-consistent ladder approximation become unreliable[4] because of the SCLA's failure to reproduce the Fermi-liquid nature of the true zero-temperature ground state of the Hamiltonian, Eq. (1). To obtain sensible results to compare with experiment in the low-temperature regime we need a way of extrapolating results to low temperatures in a way which respects the Fermi-liquid ground state. This extrapolation is possible because the failure of the SCLA is not serious until we reach temperatures below the effective Kondo temperature of the lowest-lying doublet and because of the separation of energy scales, which occurs for our choice of parameters for $CeAl_3$ and $CeCu_6$. As stated in the Introduction and explained in detail in Sec. II B, the high-lying crystal-field levels lie at energies significantly higher than the effective Kondo temperature for the low-lying doublet. At temperatures sufficiently below the crystal-field energies, we expect and find within the SCLA that the physical properties one calculates from the Hamiltonian, Eq. (1), are given by small corrections with trivial temperature dependences (constant for the susceptibility and linear in temperature for the specific heat) coming from the high-lying crystal-field states plus Kondo-like contributions coming from the lowest-lying doublet, and we expect the Kondo-like contributions to be given by the universal forms appropriate to the $S=\frac{1}{2}$ Kondo problem.[6–8] To apply the $S=\frac{1}{2}$ Kondo results to our problem we require two parameters: an effective Kondo temperature $T_0^{(2)}$ and an effective moment $\mu^{(2)}$. We obtain these two parameters, and also the background contributions, as follows: First, we use the SCLA for the Hamiltonian of Eq. (1) to obtain the specific heat and susceptibility over a wide range of temperatures. Next we observe that for T sufficiently below the crystal-field splittings ($T \leq 20$ K for parameters appropriate to $CeAl_3$ and $CeCu_6$) the specific heat we obtain, $C_{\rm SCLA}(T)$, is well fit by the sum of two terms, a linear part, AT, coming from the higher crystal-field levels and a term, $C^{(2)}_{\rm SCLA}(T)$, which is what we would obtain by applying the SCLA to a particular twofold-degenerate Kondo model, specified by a dimensionless coupling J' and a cutoff D', i.e.,

$$C_{\rm SCLA}(t)=C^{(2)}_{\rm SCLA}(T)+AT\ . \tag{11}$$

An example of such a fit is shown in Fig. 2. Note that for $J' \ll 1$ the SCLA results are universal once a temperature scale $T^{(2)}_{\rm SCLA}$ is fixed. We take the scale $T^{(2)}_{\rm SCLA}$ to be the temperature at which $C^{(2)}_{\rm SCLA}(T)$ is maximal. Further, we find that the value of $C^{(2)}_{\rm SCLA}(T^{(2)}_{\rm SCLA})$ is universal and equal to 0.21. The constant A in Eq. (11) is adjusted so that the maximum value of $C_{\rm SCLA}(T)-AT$ is equal to $C^{(2)}_{\rm SCLA}(T^{(2)}_{\rm SCLA})$. This determines unambiguously the temperature $T^{(2)}_{\rm SCLA}$, and therefore determines a set of couplings, J' and D', which yield this $T^{(2)}_{\rm SCLA}$. We believe that the values we obtain for A and $T^{(2)}_{\rm SCLA}$ are reliable because the low-temperature behavior of the SCLA solution of a model with six crystal-field levels in three well-separated doublets is essentially the same as that of the SCLA solution of Kondo model, as shown by the quality of the fits we obtain in Figs. 2 and 3. The results calculated from the SCLA are unreliable at temperatures of order $T^{(2)}_{\rm SCLA}$ or less. To obtain reliable results for the effective twofold model, we must determine the relationship between the true Kondo temperature $T_0^{(2)}$ of a twofold de-

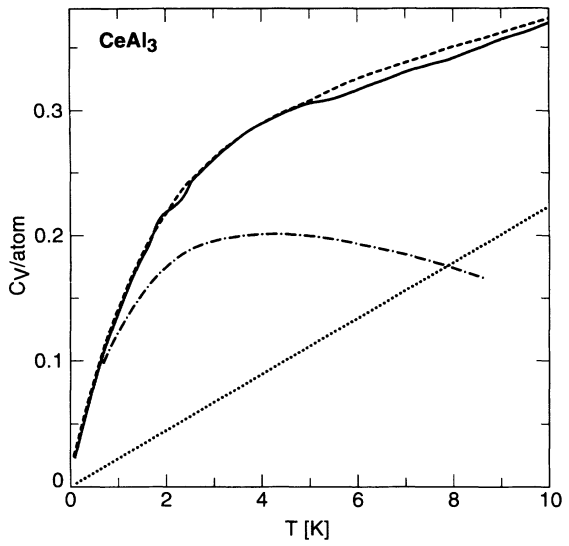

FIG. 2. Comparison of the specific heat obtained for sixfold SCLA with crystal-field splitting (solid line) to appropriately chosen twofold SCLA plus linear in temperature correction (dashed line) and the twofold SCLA (dotted and dashed line) and constant separately (dotted line). Parameters are appropriate to $CeAl_3$.

generate model with dimensionless coupling J' and cutoff D' and the $T^{(2)}_{\rm SCLA}$ of the same model. This relationship is slightly subtle because in computing a new low-energy scale from bare couplings, the way the cutoffs are implemented matters. We define $T_0^{(2)}$ via the low-temperature specific heat:[5]

$$\lim_{T\to 0}\frac{C_V(T)}{T}=\frac{\pi k_B}{6T_0^{(2)}}\ . \tag{12}$$

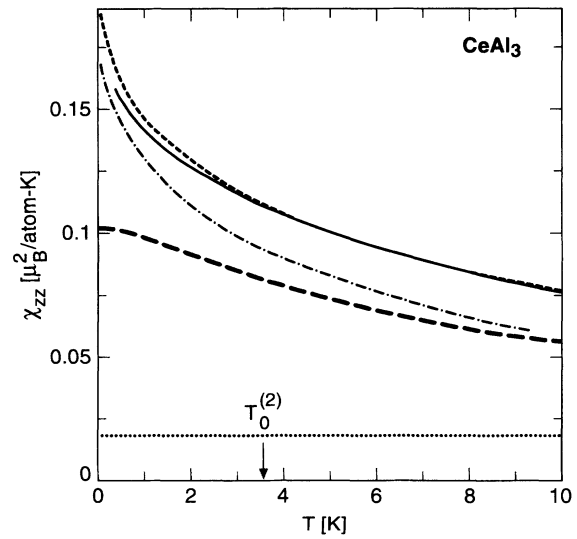

FIG. 3. Comparison of the zz susceptibility for sixfold SCLA with crystal-field splitting (solid line) to appropriately chosen twofold SCLA plus constant correction (light dashed line) to the twofold SCLA (dotted and dashed line) and constant separately (dotted line), and to the result obtained by the matching procedure described in the text (heavy dashed line). Parameters are appropriate to $CeAl_3$.

By using the relationship between T_0 and T_K,[4] and comparing with results obtained from the numerical renormalization for models with a hard bandwidth cutoff and constant density of states,[16] such as we are using, we have determined that the peak in the specific heat that results from applying the SCLA to the Kondo model is at a temperature of $1.17T_0^{(2)}=T^{(2)}_{\rm SCLA}$. The exact values chosen for D' and J' are unimportant so long as we are in the universal regime, $J'\ll 1$. Here by $T_0^{(2)}$ we mean the characteristic temperature of the Bethe-Ansatz solutions rather than Wilson's definition.[5] In support of the accuracy of this method, we note that for our choice of parameters for the cerium sites of $CeAl_3$ Kawakami *et al.*[19] have obtained a $T=0$ specific-heat coefficient of 1340 mJ/mol K, while our extrapolation scheme gives a value of 1390 mJ/mol K.

Once the temperature scale has been fixed by the location of the peak in the specific heat, we can compare the full calculated susceptibility to the SCLA calculated susceptibility of a Kondo model. The couplings and cutoff should be chosen so that the specific-heat peak occurs at the same temperature as the peak in the specific heat of the full model after the subtraction of the linear background term described above. Since the temperature dependence is now fixed, we need to further determine only an additive constant and a moment renormalization. To get the moment renormalization, one plots $[\chi_{\rm CF}(T)-\chi_{\rm CF}(T_0)]/[\chi_K(T)-\chi_K(T_0)]$, where $\chi_{\rm CF}$ is the SCLA calculated susceptibility for the actual crystal-field split model and χ_K is the SCLA calculated susceptibility for a Kondo model with the appropriately chosen temperature scale. The result should be a temperature-independent constant giving the ratio of the squares of the effective moments, $\mu^2_{\rm CF}/\mu^2_K$, and hence the moment renormalization. The constant contribution to $\chi_{\rm CF}(T)$ is then be found by plotting $\chi_{\rm CF}(T)-\mu^2_{\rm CF}/\mu^2_K\chi_K(T)$, which should be a temperature-independent constant equal to the contribution to $\chi_{\rm CF}(T)$ from the high-lying crystal-field states. We find, at $T=0$, for the parameters appropriate to $CeAl_3$, χ_{zz} of $0.10\mu_B^2/{\rm K}$ and $\chi_\perp$ of $0.045\mu_B^2/{\rm K}$, whereas the exact Bethe-ansatz results of Kawakami, Usuki, and Okiji[19] are $\chi_{zz}=0.12\mu_B^2/{\rm K}$ and $\chi_\perp=0.06\mu_B^2/{\rm K}$.

III. THE ZERO-FREQUENCY SUSCEPTIBILITY

To calculate the zero-frequency susceptibility within linear response theory, we couple the applied magnetic field to the system through the magnetic moment operator M_ν of the cerium ion

$$M_\nu=g_J\mu_B\sum_{m,m'}\langle m|J_\nu|m'\rangle f^\dagger_m f_{m'}\ , \tag{13}$$

where $\nu=x$, y, or z and J_ν is the ν component of the total angular-momentum operator, μ_B is the Bohr magneton, and g_J is the Lande g factor, equal to $\frac{6}{7}$ for the $J=\frac{5}{2}$ states of cerium. An applied field couples through a term $H_{\rm field}=\sum_\nu h^\nu M_\nu$, where h^ν is the magnetic field in the ν direction. The $\mu\nu$ component of the physical susceptibility at imaginary frequency $i\omega_n$ is obtained by taking

$\int_0^\beta d\tau \exp(i\omega_n\tau)\langle M_\mu(0)M_\nu(\tau)\rangle$. The physical susceptibility then follows from continuing to imaginary frequency and dividing by Z_λ. For the zero-frequency physical susceptibility we find the expression:

$$\chi_{\mu\nu}(0)=Z^{-1}\sum_{mm'}\int dx\,\bar{\rho}_m(x)\,\mathrm{Re}\,G_{fm'}(x)\times\langle m|J_\mu|m'\rangle\langle m'|J_\nu|m\rangle\ , \tag{14}$$

where the partition function in the $n=1$ subspace is given by

$$Z=\sum_m\int dx\,\bar{\rho}_m(x)\ . \tag{15}$$

To compute the susceptibility at low temperatures we take advantage of the fact that the results of the SCLA at temperatures far below the crystal-field splitting energies are essentially given by small, temperature-independent corrections from the higher levels plus contributions essentially the same as the results of the SCLA applied to a Kondo model with a renormalized moment. After we extract the temperature scale for this Kondo model from the specific heat as described in Sec. II C, we can determine the appropriate sizes of moment and corrections. These quantities are all that we need to compute the susceptibility in the low-temperature regime where the SCLA fails. Figure 3 shows, for the zz component of the susceptibility of $CeAl_3$, the result calculated directly from the SCLA, the match onto a SCLA-calculated Kondo susceptibility plus constant correction and the SCLA-calculated Kondo susceptibility and the constant correction separately. To extrapolate to arbitrarily low temperatures, one uses the exact Kondo results[6–8] with the appropriate moment and temperature scale $T_0^{(2)}$.[5] The inferred low-temperature susceptibility is also presented in Fig. 3.

For $CeAl_3$ the anisotropic susceptibility can be calculated straightforwardly and the results above 5 K are compared with the experimental data of Jaccard *et al.*[23] in Fig. 4. There are two primary discrepancies. First, we find no crossing of χ_{zz} and $\chi_{xx}=\chi_{yy}$ as a function of temperature, whereas the data of Jaccard *et al.*[23] show such a crossing at between 40 and 50 K. This suggests that the crystal-field level scheme we have used for $CeAl_3$ is not strictly correct, since at this high temperature the SCLA and single-site physics should give a rather good description of $CeAl_3$. This is consistent with our finding, described in Sec. V, that a strong enough Coqblin-Schrieffer coupling to produce the correct low-temperature properties for $CeAl_3$ will hybridize the crystal-field states strongly enough to destroy the two distinct inelastic peaks in the neutron scattering on whose tentative observation[17] the choice of level scheme here was based. We have not attempted to find a level scheme that reproduces the data of Jaccard *et al.*,[23] since without better guidance from neutron data the parameter space to be explored is large.

Second, we find a low temperature χ_{zz}, which is lower than that of Jaccard *et al.*[23] by about 30% at the lowest temperatures. Here there are several possible explanations for all or some of the discrepancy. First, the renormalization of the effective moment of the lowest-lying crystal-field doublet predicted by the SCLA for our parameters is too large. We find a factor of roughly 0.52 for the renormalization of the effective moment squared relative to that expected for a $|\pm\frac{3}{2}\rangle$ doublet, while from the exact results of Kawakami, Usuki, and Okiji,[19] we extract a $T=0$ renormalization of 0.6 for the effective moment squared. Second, we may be overestimating the moment renormalization due to our choice of crystal-field scheme. If the hybridization and crystal-field spacing are simultaneously increased so as to keep the effective twofold Kondo temperature the same, then the moment renormalization for the low-lying doublet should be less severe and agreement with the experimental low-temperature susceptibility would be improved. If the crystal-field levels and the hybridization were changed in a way that lowered the effective twofold Kondo temperature, then the low-temperature susceptibility would also be raised, but this is implausible in view of the relatively good agreement between our calculated specific heat and that observed experimentally. Third, there is also the possibility that the experimental data for χ_{zz} are sufficiently uncertain that the difference is not significant. Weak ferromagnetic correlations among cerium ions would raise the low-temperature uniform susceptibility relative to the specific heat, as would a slight admixture of the $J=\frac{7}{2}$ cerium states. A remote possibility is that the lowest crystal-field doublet is actually the $|\pm\frac{5}{2}\rangle$. This would increase the low temperature χ_{zz} by nearly $\frac{25}{9}$ at the lowest temperatures and would require substantial corrections of

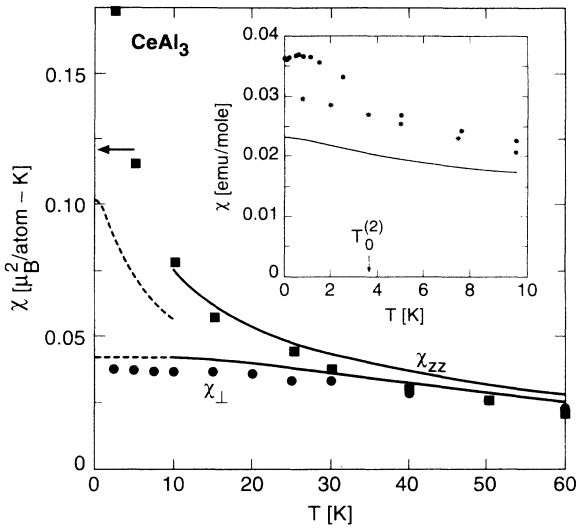

FIG. 4. Experimental results of Jaccard (Ref. 23) (χ_{zz}=squares and $\chi_\perp$=dots) for $CeAl_3$ single-crystal, SCLA susceptibility (line) above 10 K and susceptibility extrapolation (dashed line) from SCLA results for temperatures below 10 K. The arrow marks the $T=0$ Bethe-ansatz result of Kawakami, Usuki, and Okiji (Ref. 19). Inset: comparison of the polycrystalline susceptibility of $CeAl_3$ from Ott *et al.* (Ref. 25) (dots) and Edelstein (Ref. 26) (stars) to the angle averaged results for the susceptibility obtained with our matching procedure. The effective Kondo temperature $T_0^{(2)}$ was 3.6 K. Parameters are appropriate to $CeAl_3$.

the opposite sign from other sources to agree better with the experiment than the choice of the $|\pm\frac{3}{2}\rangle$ states. On the basis of neutron-scattering Goremychkin, Natkaniec, and Mühle[28] have proposed that the lowest crystal-field doublet is actually the $|\pm\frac{1}{2}\rangle$. This proposal was made before the availability of single-crystal susceptibility data and, in the face of the anisotropy of the low-temperature single-crystal susceptibility, we do not think that the proposal of Goremychkin, Natkaniec, and Mühle[28] can be made consistent with the data.

The experimental susceptibility for polycrystalline samples is compared with the results inferred from the SCLA in the inset to Fig. 4. The temperature dependence agrees qualitatively with the experiments except for the weak anomaly occurring below 1 K. This anomaly occurs at a temperature below the lowest single-site energy scale and most likely involves intersite correlation effects. The theoretical susceptibility is consistently smaller than the experimental observation; however, the magnitudes of suscepibilities are difficult to measure experimentally, and those of Ott *et al.*[25] and Edelstein[26] disagree substantially, so it is not clear if this difference is significant. We have already discussed possible explanations.

As mentioned earlier, for $CeCu_6$, the complicated crystal structure prevents us from computing the crystal-field eigenfunction and, hence, the susceptibility. Instead we choose matrix elements which reproduce the qualitative features of the anisotropic static susceptibility as measured by Onuki, Shimizu, and Komatsubara.[27] The qualitative features, which we reproduce with our choice, are the large anisotropy at low temperatures of the susceptibility (a factor of ~ 10), the nonmonotonic temperature dependence of the susceptibility for fields in the $\hat{b}$ direction, and the crossing at a temperature of several tens of kelvins of the suscepibilities for field applied in the $\hat{b}$ and $\hat{c}$ directions. We do not attempt a quantitative low-temperature comparison of the theoretical and experimental susceptibilities, since this would require a precise determination of the wave functions of the crystal-field eigenstates. To achieve our qualitative description, we define a separate set of spin quantization axes for each cerium ion. With respect to these axes, we take the crystal-field eigenstates for each cerium ion as follows: The low-lying doublet consists of the $J^z=\frac{5}{2}$ ($|\frac{5}{2}\rangle$) and $J^z=-\frac{5}{2}$ ($|-\frac{5}{2}\rangle$) states, the first excited doublet contains the states $1/\sqrt{s}$ ($|\frac{3}{2}\rangle-|-\frac{1}{2}\rangle$) and $1/\sqrt{2}$ ($|-\frac{3}{2}\rangle-|\frac{1}{2}\rangle$), while the highest doublet contains the states $1/\sqrt{2}$ ($|\frac{3}{2}\rangle+|-\frac{1}{2}\rangle$) and $1/\sqrt{2}$ ($|-\frac{3}{2}\rangle+|\frac{1}{2}\rangle$). This allows us to compute the anisotropic susceptibility of the individual cerium ions with respect to axes whose orientations we leave unspecified. To take into account orientation effects, we take the susceptibility along a given crystallographic symmetry axis to be simply a weighted average of the susceptibilities we compute for a single cerium ion in various directions:

$$\chi_a(T)=\cos 2(\theta_{ax})\chi_{xx}(T) + \cos^2(\theta_{ay})\chi_{yy}(T)+\cos^2(\theta_{az})\chi_{zz}(T)\ , \quad (16)$$

$$\chi_b(T)=\cos^2(\theta_{bx})\chi_{xx}(T) + \cos^2(\theta_{by})\chi_{yy}(T)+\cos^2(\theta_{bz})\chi_{zz}(T)\ , \quad (17)$$

$$\chi_c(T)=\cos^2(\theta_{cx})\chi_{xx}(T) \cos^2(\theta_{cy})\chi_{yy}(T)+\cos^2(\theta_{cz})\chi_{zz}(T)\ , \quad (18)$$

where θ_{ax} is the angle between the local $\hat{x}$ quantization axes and the crystallographic $\hat{a}$ direction, etc. This procedure allows us to explain qualitatively many of the features of the experimental anisotropic susceptibility for $CeCu_6$.

The extreme anisotropy between the susceptibility in the different crystallographic symmetry directions is naturally explained by taking the lowest-lying doublet to have no matrix elements for J^+ and J^-, where these operators are defined with respect to some local quantization axis. The results for the susceptibility of a single cerium ion without any angle averaging or weighting factors are presented in the inset to Fig. 5. If one takes angular weighting factors such that the local quantization axes are nearly parallel to the crystalographic $\hat{c}$ direction, then this leads to χ_c being much larger than χ_a and χ_b, as observed. The low-temperature maximum in χ_a can also be explained straightforwardly. For no matrix elements for J^+ and J^- within the low-lying doublet, χ_{xx} and χ_{yy} both turn down at low temperatures (see the inset to Fig. 5). If the weighting for the χ_{zz} contribution to χ_b is sufficiently small, then this downturn will cause a downturn in χ_b at an intermediate temperature, followed by an upturn at sufficiently low temperatures, provided that χ_{zz} is sufficiently larger than χ_{xx} and χ_{yy} at low temperatures. The downturn is absent in χ_a because the

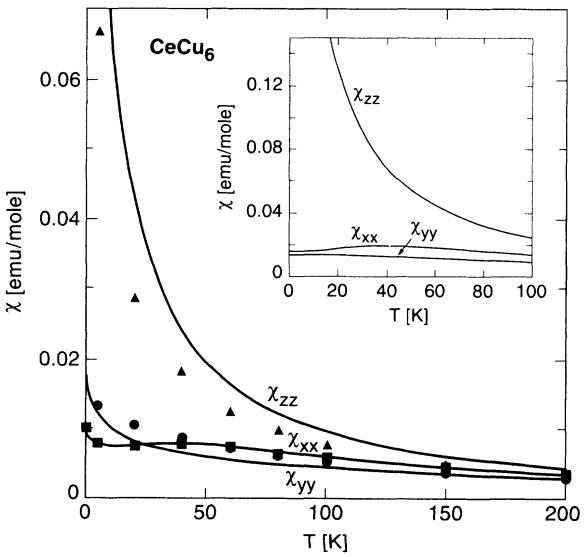

FIG. 5. Experimental results (dots) of Onuki, Shimizu, and Komatsubara (Ref. 27) for single-crystal $CeCu_6$ together with our theoretical results. Circular dots are the $\hat{a}$ direction, square dots are the $\hat{b}$ direction, and triangular dots are the $\hat{c}$ direction. Inset: calculated susceptibility for a single cerium ion in the $CeCu_6$ environment. The $\hat{z}$ axis is the quantization axis for the local moment.

weighting factor determining the χ_{zz} contribution to χ_a is sufficiently large to mask the downturn in χ_{xx} and χ_{yy}. The difference in these weighting factors plus the low-temperature dominance of χ_{zz} over χ_{xx} and χ_{yy} also explains the crossing of χ_a and χ_b. At high temperature the contributions from the higher-lying doublets make χ_b larger than χ_a, whereas at low temperature the contribution from χ_{zz} dominates and χ_a is larger than χ_b. One can see by examining the main part of Fig. 5 that the behavior of the actual system is reproduced qualitatively quite well by our choice of parameters. There is some discrepancy in magnitude between the calculated and measured susceptibilities, with the calculated susceptibilities all being somewhat larger than those experimentally observed. However, the general temperature dependence is well reproduced. Also, the temperature for the experimental crossing of χ_a and χ_b differs from that which we calculate for our choice of crystal-field wave functions. However, the position of the crossing is fairly sensitive to the exact choice of wave functions, so this discrepancy most likely indicates that while our explanation of its origin is essentially correct, we have not chosen our wave functions precisely enough to reproduce the crossing quantitatively.

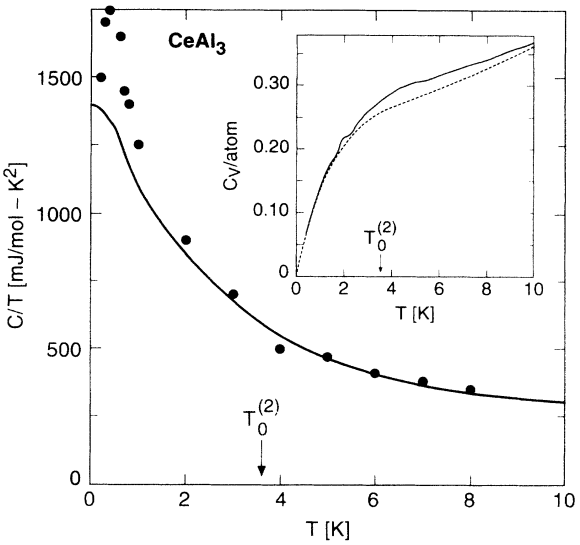

FIG. 6. Experimental specific heat divided by temperature for $CeAl_3$ (dots) vs the theoretical result obtained by matching procedure described in the text. The effective Kondo temperature $T_0^{(2)}$ was 3.6 K. Note that the low-temperature peak is not well reproduced. Inset: Comparison of the SCLA specific heat (solid line) to the result (dashed line) obtained by the matching procedure described in the text.

IV. THE SPECIFIC HEAT

At temperatures above a few kelvin, the specific heat within our model is easily calculated from the partition function defined in Eq. (15)

$$C_V = T\frac{\partial^2}{\partial T^2}\{T\ln[Z(T)]\} . \tag{19}$$

To take the derivatives numerically we use cubic spline interpolation on the partition function calculated at a number of temperatures to define $Z_{\text{interpolated}}$ and then differentiate $Z_{\text{interpolated}}$ exactly. This approach encounters difficulties at low temperatures due both to the difficulties of calculating the derivatives in this manner and to the failure of the SCLA at low temperatures. To circumvent the second problem we apply the matching procedure described in Sec. II C (Ref. 16) and SCLA results for the same Kondo model. Figure 3 shows the SCLA calculated specific heat at low T, the matching of this with a constant plus a SCLA-calculated Kondo model specific heat, and the linear in T contribution and SCLA Kondo contributions separately. The inset to Fig. 6 shows the SCLA-calculated specific heat at low T and the actual low-temperature specific heat we obtain from our extrapolation scheme.

The calculated specific-heat coefficient, $\gamma(T) = C_V(T)/T$, for $CeAl_3$ is compared with experiment in Fig. 6. The general agreement is good, the only marked difference being the inability of a single-site model to reproduce the feature found below one kelvin in the experimental data. This feature occurs at a temperature (<1 K) lower than the lowest temperature scale for our independent-ion model (for our parameters $T_K^{(2)}=3.2$ K for $CeAl_3$) and must involve additional physics. Additionally, the specific-heat coefficient we find is larger at $T=0$ than the experimental result, suggesting that the $T_K^{(2)}$ we found may be too small. However, the susceptibility we found is slightly smaller than the experimental result in contradiction to this idea. We cannot determine whether this deviation is the result of out neglect of cerium-cerium correlations or of the approximations we have made in treating our single ion Hamiltonian. However, the $T=0$ agreement between the Bethe-ansatz results of Kawakami, Usuki, and Okiji[19] with $C_V(0)=1340$ mJ/mol K and our SCLA with low-temperature extrapolation result with $C_V(0)=1390$ mJ/mol K suggests that our approximate methods are reasonably accurate for the single-site physics.

Since the specific heat depends only on the energy spacings of the doublets, not their wave functions, computing the specific heat for $CeCu_6$ poses no problems. The results we obtain for $CeCu_6$ are compared with experiment in Fig. 7. For this case the agreement is good at temperatures below about 8 K. Above this temperature the experimental $C_V(T)/T$ curve turns upwards, probably due to contributions from sources other than the cerium ions. This agreement at low temperatures suggests that the feature found in $CeAl_3$ below one K is not a generic feature of Kondo lattice systems. If so, it appears that the specific heat at low temperatures for Kondo lattice materials may sometimes be well described using only single-site physics.

V. THE IMAGINARY SUSCEPTIBILITY, $\chi''(\omega)$

The imaginary part, $\chi''(w)$, of a cerium ion's susceptibility at finite temperature and frequency can also be calculated easily from the solution of the SCLA equations and is[2]

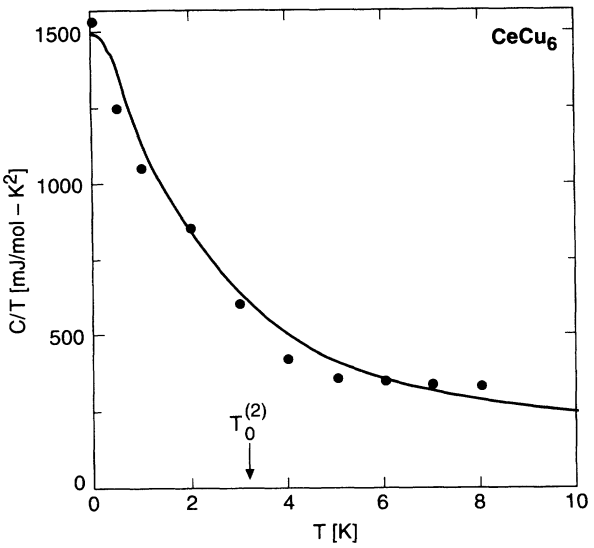

FIG. 7. Experimental specific heat divided by temperature for $CeCu_6$ (dots) vs theoretical result obtained by matching procedure described in the text. The effective Kondo temperature $T_0^{(2)}$ was 3.2 K. The agreement is worse for $T > 8$ K.

$$\chi''_{\mu\nu}(\omega) = Z^{-1}\pi(g_J\mu_B)^2[1-\exp(-\beta\omega)] \times \sum_{m_1,m_2} \langle m_1|J_\mu m_2\rangle\langle m_2|J_\nu|m_1\rangle \times \int dx\, \bar{\rho}_{m_1}(x)\rho_{m_2}(x+\omega)\,, \quad (20)$$

where ρ is defined in Eq. (7) and $\bar{\rho}$ in (9). This quantity is of experimental interest, since the neutron-scattering cross section σ, because of the dipolar interaction of the neutrons magnetic moments with the cerium ions' moments is related to χ'' by

$$\frac{d^2\sigma}{d\Omega\, d\omega} \propto [1-\exp(-\beta\omega)]^{-1} \sum_{\mu,\nu} \left(\delta_{\mu\nu} - \frac{q_\mu q_\nu}{q^2}\right) \chi''_{\mu\nu}(\omega)\,. \quad (21)$$

Within our approximation the q dependence in the scattering cross section arises entirely from form factors, since all correlations among the cerium ions are neglected.

We present the calculated susceptibilities, divided by the thermal factor $1-\exp(-\beta\omega)$ for $CeAl_3$ in Figs. 8(a) and 8(b). The matrix elements used are those of Sec. III and are fixed by the symmetry of the cerium ion's crystal-field environment. The crystal-field levels are sufficiently broadened that only a single inelastic peak is visible, in contradiction to the original neutron work of Murani, Khorn, and Buschow[17] on which our crystal-field scheme was based, but in agreement with the more recent work of Goremychkin, Natkaniec, and Mühle.[28]

The possibility that the lowest-lying doublet is the $\pm\frac{1}{2}$ doublet has been raised based on neutron-scattering results by Goremychkin, Natkaniec, and Mühle in order to account for the presence of only a single inelastic peak; however, the anisotropic single-crystal static susceptibility is most naturally explained with a ground-state doublet with vanishing matrix elements for J^x and J^y, excluding the $\pm\frac{1}{2}$ doublet. Further, the magnitude of the anisotropic susceptibility would vary by a factor of $\frac{1}{9}$ or $\frac{25}{9}$ if the lowest-lying doublet were changed from $\pm\frac{3}{2}$ to the $\pm\frac{1}{2}$ or $\pm\frac{5}{2}$, respectively. This would not agree with the experimentally observed magnitudes.[23] The competition between the Kondo and crystal-field effects can account for both the presence of a single inelastic peak and the magnitude and anisotropy of the susceptibility naturally. We find no upturn in the scattering at low frequencies, the quasielastic contribution manifesting itself in a low-energy shoulder in the scattering intensity in agreement with the Goremychkin data.

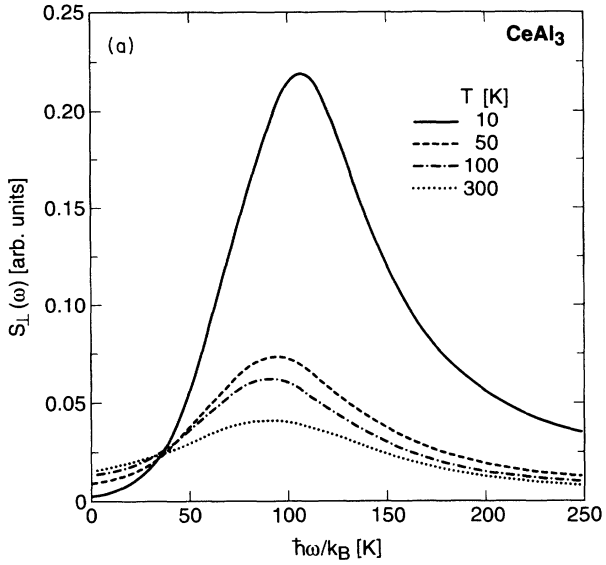

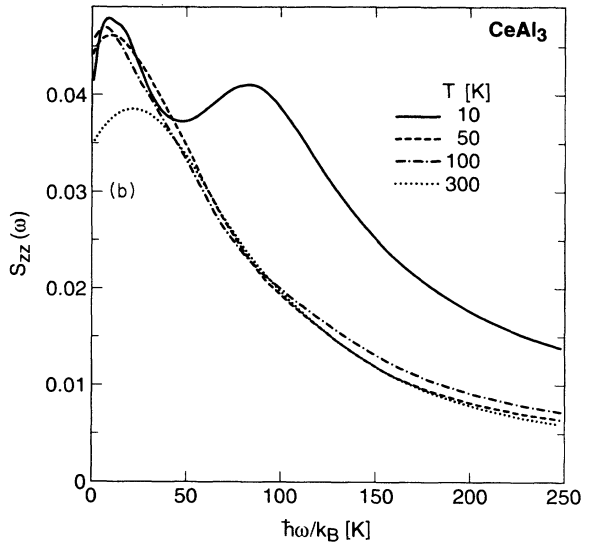

FIG. 8. $S_{\perp,zz}(\omega) = [1-\exp(-\beta\omega)]^{-1}\chi''_{\perp,zz}(\omega)$ for $CeAl_3$ parameters. The solid line is $T = 10$ K, the dashed $T = 50$, the dotted and dashed $T = 100$, and the dotted $T = 300$. Vertical axis units are arbitrary.

For $CeCu_6$ we use the choice of matrix elements de-

scribed in Sec. III, omitting the angular weighting factors for convenience, and find the susceptibilities depicted in Figs. 9(a)–9(c). The data are in reasonable agreement with the neutron scattering work of Walter, Wohlleben, and Fisk[21] and Goremychkin and Osborn.[22]

VI. TEMPERATURE-DEPENDENT RESISTIVITY

Following Kashiba *et al.*[29] we now calculate the temperature dependence of the anisotropic resistivity for $CeAl_3$ and $CeCu_6$. Under the assumption of free-electron-like dispersion, the Boltzmann form for the conductivity is

$$\sigma_{\mu\nu}=-\frac{e^2}{m}\sum_{\sigma}\int dk\int\frac{d\Omega_k}{4\pi}k_\mu k_\nu\tau_\sigma(k)\left[-\frac{\partial f(E_k)}{\partial E_k}\right]. \tag{22}$$

For temperatures small compared to the bandwidth, we can replace this with

$$\sigma_{\mu\nu}=-\frac{e^2}{m}N(0)\sum_{\sigma}\int_{-D}^{D}dE\int\frac{d\Omega_k}{4\pi}k_\mu k_\nu\tau_\sigma(\mathbf{k})\times\left[-\frac{\partial f(E)}{\partial E}\right], \tag{23}$$

which is suitable for calculation within the SCLA. Now $\tau_\sigma(k)$ is given by[29]

$$\tau_\sigma^{-1}(\mathbf{k})=-2c_i\sum_m|\langle\mathbf{k},\sigma|k,m\rangle|^2\,\mathrm{Im}T_m(E_k), \tag{24}$$

where c_i is the concentration of scatterers and $\mathrm{Im}T_m$ is given in the SCLA by

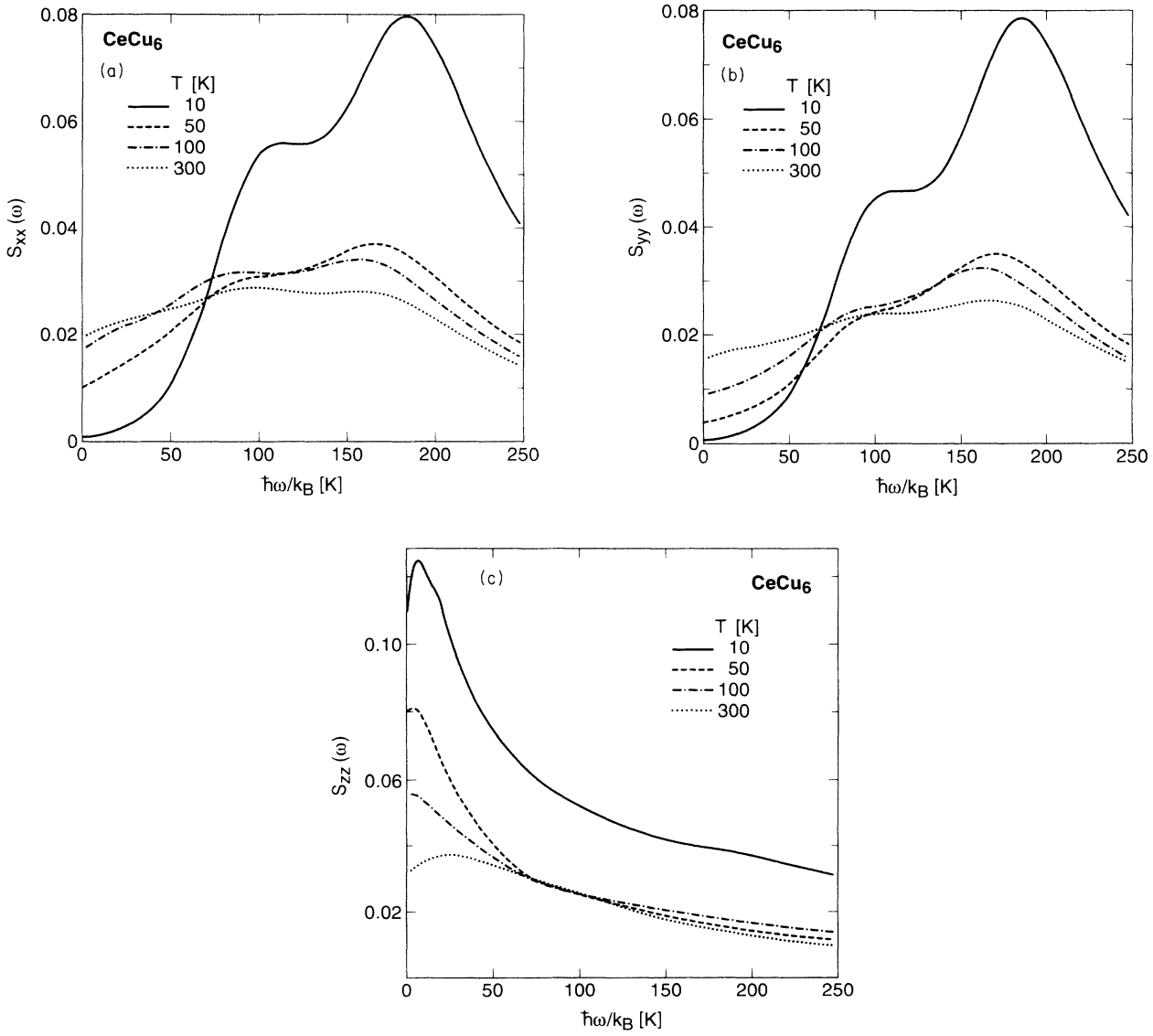

FIG. 9. $S_{ii}(\omega)=[1-\exp(-\beta\omega)]^{-1}\chi''_{ii}(\omega)$ for $CeCu_6$ parameters ($i=x,y,z$). The solid line is $T=10$ K, the dashed $T=50$, the dotted and dashed $T=100$, and the dotted $T=300$. Vertical axis units are arbitrary.

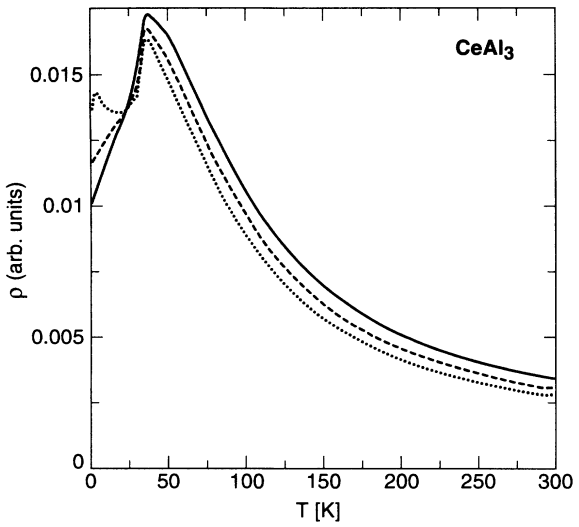

FIG. 10. Anisotropic and angle-averaged resistivities computed with the SCLA for $CeAl_3$. The vertical axis is resistivity is in arbitrary units, and the horizontal axis is temperature in kelvin. The dashed line is the averaged resistivity, $\bar{\rho}^{-1}=\frac{1}{3}(2\rho_{\perp}^{-1}+\rho_{zz})$. The solid line is ρ_{zz} and the dotted is $\rho_{\perp}$. We have not presented results for $T \lesssim T_0^{(2)}$ because the SCLA is not valid there, and we have not obtained resistivity results from our matching procedure.

$$\mathrm{Im}T_m(\omega)=Z^{-1}\pi J\int dx\,\bar{\rho}_m(x)\eta(x-\omega) +\rho_m(x)\eta(\bar{x}-\omega)\ . \tag{25}$$

The dependence of the resistivity on wave vector enters through the matrix elements $\langle \mathbf{k},\sigma|k,m\rangle$. For $CeAl_3$, we can compute these explicitly for our choice of crystal-field level scheme. Our results for the anisotropic and angle-averaged resistivities are shown in Fig. 10.

First, let us discuss the polycrystalline resistivity. Our results agree qualitatively with the temperature dependence seen experimentally. There is deviation at high temperatures, where we predict a resistivity falling faster with increasing temperature. This may be due to inadequacies of our model for the physics of the cerium ions or may be due to the scattering from phonons contributing to the temperature dependence of the resistivity. In general, high temperature implies the destruction of correlations and hence an increased validity for a single-site model and, simultaneously, an increase in the effective degeneracy for the cerium ions, which should increase the accuracy of the SCLA. For these reasons we do not believe that the discrepancies at high temperature are due to flaws in the way our model treats the physics of the cerium ions. In support of this we note that a similar discrepancy occurs for $CeCu_6$ if we compare to the raw data of Onuki, Shimizu, and Komatsubara.[27] However, Onuki, Shimizu, and Komatsubara also measured the resistivity for $LaCu_6$ (identical structure but with cerium replaced by lanthanum) to allow the subtraction of scattering from phonons and found a linear contribution to $\rho(T)$ for $LaCu_6$ of the right size to essentially remove the discrepancy.

There is qualitative agreement in an intermediate temperature range, which extends down to temperatures of order a few kelvin. At lower temperatures the resistivity in our calculation saturates, as it must for a model with only single-site physics, in which there is no possibility of coherence. The actual behavior of $CeAl_3$ is Fermi-liquid-like at low T with $\rho(T)\sim\rho_0+\alpha T^2$ at low T and ρ_0 tending to zero in good crystals. It is important to note that the temperature where significant deviations from the temperature dependence of our model occur is of order a few degrees kelvin, not tens of degrees kelvin. We conclude that the maximum in the experimental resistivity for polycrystalline $CeAl_3$ frequently associated with the onset of coherence and occurring at approximately 30 K,[24] far above the effective Kondo temperature of the low-lying doublet, can be reproduced fairly well by a single-site model in which there is no attempt to take coherence into account. This suggests that the physics of the resistivity downturn in $CeAl_3$ at this temperature has more to do with crystal-field effects than with the overlapping of the Kondo screening clouds and that the energy scale for coherence is not as high as one would conclude from a naive examination of the temperature-dependent resistivity.

Now we turn to the anisotropy at the resistivity. The most striking feature is that the anisotropy of the single crystal resistivity is much stronger in the experimental data[23] than in our calculation. Since this effect persists up to quite high temperatures, where single-site physics and the SCLA should both be reasonable approximations, we conclude that much of the anisotropy must be a consequence of things other than coherence, which our calculation has neglected. In particular, anisotropy in the band structure has been completely neglected in our calculation and could result in substantial anisotropy in the resistivity.

For $CeCu_6$ the differing orientations of the inequivalent cerium ions make the matrix elements needed in Eq. (24), $\langle \mathbf{k},\sigma|k,m\rangle$, difficult to compute, even if we assume a crystal-field level scheme for the cerium ions. We therefore make the following approximation to get an idea of the qualitative behavior for $CeCu_6$: We treat all the cerium ions as having the same orientation and use the level scheme proposed in Sec. III. This should give a reasonable picture, since the angular weighting factors used in that section implied that the orientations of the cerium atoms were such that their local quantization axes were close to parallel to the $\hat{c}$ direction and the results calculated for σ_{xx} and σ_{yy} are nearly identical owing to the strong hybridization for the crystal-field levels and the vanishing of J^+ and J^- in the lowest-lying doublet. The imprecise treatment of the conductivities for directions perpendicular to $\hat{c}$ is thus not particularly important, while the treatment of the conductivity in the $\hat{c}$ direction should be qualitative reasonable; however, our choice will produce the maximum possible conductivity in the $\hat{c}$ direction, since we have aligned all of the quantization axes in exactly this direction and chose for the ground-state doublet the $|\pm\frac{5}{2}\rangle$ states, which are least effective at scattering electrons moving in the $\hat{c}$ direction, so we are definitely overestimating the conductivity in this direction, and the conductivity anisotropy as a result.

Our results for the anisotropic and angle-averaged resistivities for $CeCu_6$ are shown in Fig. 11. The agreement between angle averaged resistivity and experimental results for this quantity is rather poor, since we find a peak in the resistivity at a temperature of around 50 K as opposed to below 20 K, as seen experimentally. This may be due to the extremely approximate matrix elements we have used for the conductivity calculation for $CeCu_6$, but we think it unlikely because an angle-averaged quantity like the resistivity should be relatively insensitive to matrix element choices. Since coherence effects should only increase the temperature at which the resistivity turns down, they do not appear as likely candidates for explaining this discrepancy. Magnetic correlation appears a more probable candidate for explaining these deviations from single-site behavior.

There is also a discrepancy at high temperatures in the rate of decrease of the resistivity with temperature, but here again we expect this to be due to the contributions of other scattering mechanisms to the resistivity. The data of Onuki, Shimizu, and Komatsubara[27] show a nearly linear in T resistivity for $LaCu_6$ with a magnitude at 300 K over half that of $CeCu_6$, suggesting that other scattering mechanisms, presumably phonons, are important at these temperatures and that their temperature dependence is predominantly of the opposite sign of the magnetic scattering from the cerium ions, so as to produce a much weaker, nonmonotonic temperature dependence in the total resistivity.

The agreement with the anisotropic resistivity is not very good. The extremely approximate choice of matrix elements and our total neglect of band-structure effects in calculating $\rho(T)$ make any comparison with experiment very much qualitative. The conductivity is highest in the $\hat{c}$ direction, where the magnetic susceptibility is largest. This is to be expected, since the large susceptibility results from a low-lying doublet with a sizable admixture of the states with large values for $\langle J^c \rangle$. This doublet will strongly scatter electrons in partial wave channels with large value overlaps with the large J^c states; these are predominantly electrons moving in the plane perpendicular to $\hat{c}$, so the resistivity is lower in the $\hat{c}$ direction. The theoretical anisotropy is much larger than the experimental ($\sim$5:1 versus $\sim$2:1), but this is because we have chosen the most anisotropic possible matrix elements for the low-lying doublet. The susceptibility data require very large matrix elements of J^z within this doublet, but the resistivity is sufficiently sensitive to the exact choice of doublet wave function that changes consistent with the required large matrix elements for J^z are probably sufficient to remove the discrepancy. We have not explored this point in detail due to the large parameter space resulting from the complicated crystalline structure of $CeCu_6$. One point of agreement between our calculation and experiment is that the $\hat{c}$ direction resistivity ρ_c remains significantly smaller than the resistivities in the $\hat{a}$ and $\hat{b}$ directions at temperatures well above that for which ρ_a and ρ_b have become essentially identical.

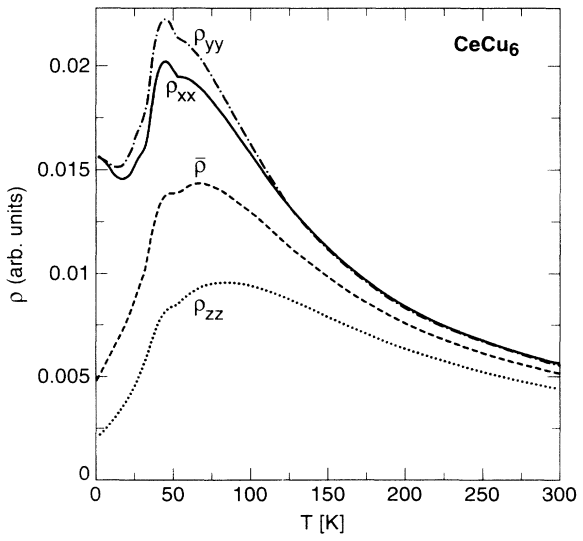

FIG. 11. Anisotropic and angle-averaged resistivities computed with the SCLA for $CeCu_6$. The vertical axis is resistivity in arbitrary units, and the horizontal axis is temperature in kelvin. The dashed line is the averaged resistivity, $\bar{\rho}^{-1} = \frac{1}{3}(\rho_{xx}^{-1} + \rho_{yy} + \rho_{zz})$. The solid line is ρ_{xx}, dashed and dotted is ρ_{yy}, and the dotted line is ρ_{zz}. We have not presented results for $T \lesssim T_0^{(2)}$ because the SCLA is not valid there, and we have not obtained resistivity results from our matching procedure.

The disagreements between our calculation and the experimental results are most striking at low temperatures. The temperatures observed experimentally for the resistivity maxima in the various directions are significantly off from what we expect based on our crystal-field scheme. This discrepancy is not easily explained by the approximate nature of our matrix elements, since we find the theoretical downturn at roughly the same temperature for all directions, and experimentally it occurs far below this temperature, with the downturn in the $\hat{a}$ direction coming at a temperature comparable to our effective Kondo temperature for the low-lying doublet. The behavior of ρ_a is exceptional, and is probably due to the matrix elements entering into the conductivity in that direction being such that the conductivity is quite insensitive to the high-lying crystal-field states and their freezing out. In this case, the downturn of $\rho_a(T)$ is actually measuring the true coherence temperature for this material, rather than effects related to crystal fields. That ρ_b and ρ_c have their downturns at temperatures so far below the crystal-field energies we have used based on neutron-scattering data could result from our model if there was a much closer competition between the Coqblin-Schrieffer interaction and the crystal-field physics than we have assumed here, or if all the energy scales, crystal field and sixfold Kondo, were substantially lower. This is difficult to reconcile with the good agreement found with the low-temperature specific-heat and suggests that the problems with applying a single-site model to $CeCu_6$ may be manifesting themselves in this way. One expects coherence effects to lead to an increase in the temperature at which the resistivity maximum occurs, not a decrease; therefore, it seems more likely that magnetic correlations between cerium ions are playing some role in the temper-

ature dependence of the resistivity and shifting the maximum in ρ to a lower temperature. In general, the resistivity data are substantially less well explained within the single-site physics of our model than are the thermodynamic quantities such as specific heat and magnetic susceptibility.

VII. DISCUSSION AND CONCLUSIONS

It has been suggested that heavy-fermion compounds such as $CeAl_3$ and $CeCu_6$, while not known to order magnetically, may have strong enough antiferromagnetic correlations for the thermodynamic properties to deviate markedly from what one expects within an independent-ion model.[30] In particular, one expects soft antiferromagnetic modes to contribute strongly to the low-temperature specific heat, helping to explain its large value, without enhancing the bulk susceptibility. We find no evidence in the case of $CeCu_6$ that the low-temperature behavior of these two quantities deviates significantly from the predictions of an independent ion model, once crystal-field effects have been properly taken into account. We have been forced to approximate the matrix elements needed to calculate the bulk susceptibility in $CeCu_6$ and cannot rule out the possibility that antiferromagnetic correlations are important for the thermodynamic properties, but the experimental data certainly do not require such an explanation. We do find evidence that the temperature dependence of the resistivity for this material is not well explained within a single-site model such as ours, and this may indicate a role for magnetic correlations.

For $CeAl_3$, the independent-ion model does a reasonable job of reproducing the anisotropic susceptibility down to the lowest-temperature experiments (3 K) of which we are aware. The angle averaged susceptibility agrees reasonably well with experiment below 10 K with two exceptions: It is consistently slightly lower than the experimental values, in contradiction to what one expects from antiferromagnetic correlations, and it does not contain the low-temperature anomaly found below 1 K experimentally. The anisotropic susceptibility we calculated also agrees well, except at the lowest temperatures. The experimental results are again higher than the theoretical, and the discrepancy does not suggest strong antiferromagnetic correlations. The resistivity we calculate for $CeAl_3$ is not nearly as anisotropic as observed experimentally, but does have a similar temperature dependence down to less than 10 K. This suggests that the temperature at which coherence effects become noticeable in the resistivity is of order a few kelvins, rather than tens of kelvins. The specific heat is well reproduced down below 10 K with the prominent exception of the low-temperature maximum in C_V/T. We believe that no realistic single-site model can explain this anomaly, since the temperature at which it occurs is well below the lowest natural single-ion energy scales. Further, no such anomalies occur for $CeCu_6$, despite the fact that its single-site energy scales are quite similar to those of $CeAl_3$. It has been suggested on the basis of muon,[31] NMR,[32] and resistivity[23] data that $CeAl_3$ undergoes antiferromagnetic ordering at $T_N \sim 1.6$ K. This temperature is in rough agreement with the characteristic temperature for the specific-heat anomaly. Such a magnetic transition is clearly the most likely explanation of the anomalies occurring for $CeAl_3$. If so, their absence for $CeCu_6$ suggests that strong magnetic correlations are not a prerequisite for the high γ's of Kondo lattice materials.

In general, we find the thermodynamic quantities to be surprisingly well described by our single-site model with no evidence that antiferromagnetic correlations are essential to understanding these quantities in $CeCu_6$ or in $CeAl_3$ above 2 K. Transport properties are much less well described by our single-site model and require some additional physics for detailed understanding in both $CeCu_6$ and $CeAl_3$.

*Present address: NEC Research Institute, 4 Independence Way, Princeton, NJ 08540.

[1]B. Coqblin and J. R. Schrieffer, Phys. Rev. **185**, 847 (1968).
[2]S. Maekawa *et al.*, J. Phys. Soc. Jpn. **54**, 1955 (1984).
[3]A. A. Abrikosov, Physics **2**, 5 (1965).
[4]N. E. Bickers, Rev. Mod. Phys. **59**, 845 (1987).
[5]Here we use T_0 as defined in Ref. 6 so that for an N-fold-degenerate multiplet $\gamma=(N-1)\pi k_B/6T_0$.
[6]V. T. Rajan, Phys. Rev. Lett. **51**, 308 (1983).
[7]P. Schlottman, Z. Phys. B **54**, 207 (1984).
[8]P. B. Wiegmann, E. T. Ogievetskii, and A. M. Tsvelik, JETP Lett. **37**, 693 (1983).
[9]G. R. Stewart, Rev. Mod. Phys. **56**, 755 (1984).
[10]P. Coleman, Phys. Rev. B **29**, 3035 (1984).
[11]A. Zawadowski and P. Fazekas, Z. Phys. **226**, 235 (1969).
[12]J. L. Black *et al.*, Phys. Rev. B **26**, 1559 (1983).
[13]N. E. Bickers, D. L. Cox, and J. W. Wilkins, Phys. Rev. B **36**, 2036 (1987).
[14]Y. Kuramoto, Z. Phys. B **53**, 37 (1983).
[15]F. C. Zhang and T. K. Lee, Phys. Rev. B **30**, 1556 (1984).
[16]H. R. Krishna-murthy, J. W. Wilkins, and K. G. Wilson, Phys. Rev. B **21**, 1003 (1980).
[17]A. P. Murani, K. Knorn, and K. H. J. Buschow, *Crystal Field Effects in Metals and Alloys,* edited by A. Furrer (Plenum, New York, 1977), p. 121.
[18]The $T_0^{(6)}$ was obtained from identifying the temperature of the maximum of the NCA-calculated $C_V(T)$ with $0.3T_0^{(6)}$, the temperature of the maximum in the exact solution of Ref. 6.
[19]N. Kawakami, T. Usuki, and A. Okiji, J. Phys. Soc. Jpn. **58**, 1427 (1989).
[20]H. A. Bethe, Z. Phys. **71**, 205 (1931).
[21]U. Walter, D. Wohlleben, and Z. Fisk, Z. Phys. B **62**, 325 (1986).
[22]E. A. Goremychkin and R. Osborn, Phys. Rev. B **47**, 14 580 (1993).
[23]D. Jaccard *et al.*, J. Magn. Magn. Mater. **76&77**, 155 (1988).
[24]H. R. Ott, H. Rudiger, Z. Fisk, and J. L. Smith, Physica B+C **127B**, 359 (1984).

[25]H. R. Ott *et al.*, Phys. Rev. Lett. **35**, 1779 (1975).
[26]A. Edelstein, Solid State Commun. **15**, 81 (1974).
[27]Y. Onuki, Y. Shimizu, and T. Komatsubara, J. Phys. Soc. Jpn. **54**, 304 (1985).
[28]E. A. Goremychkin, I. Natkaniec, and E. Mühle, Solid State Commun. **64**, 553 (1987).
[29]S. Kashiba, S. Maekawa, S. Takahashi, and M. Tachiki, J. Phys. Soc. Jpn. **55**, 1341 (1986).
[30]C. M. Varma, *Physical Phenomena at High Magnetic Fields,* edited by E. Manousakis, P. Schlottman, P. Kumar, K. S. Bedell, and F. M. Mueller (Addison-Wesley, Redwood City, 1992), p. 156.
[31]S. Barth *et al.*, Phys. Rev. Lett. **59**, 2991 (1987).
[32]H. Nakamura, Y. Kitaoka, K. Asayama, and J. Flouquet, J. Magn. Magn. Mater. **76-7**, 465 (1988).